

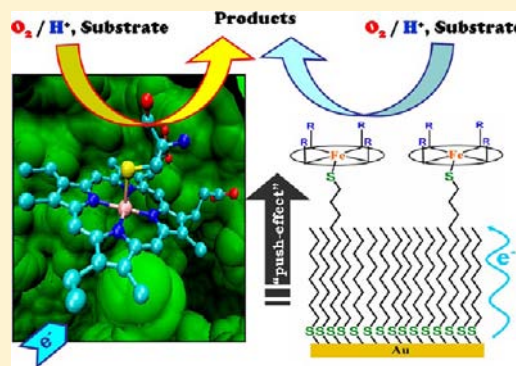
Resonance Raman and Electrocatalytic Behavior of Thiolate and Imidazole Bound Iron Porphyrin Complexes on Self Assembled Monolayers: Functional Modeling of Cytochrome P450

Kushal Sengupta, Sudipta Chatterjee, Subhra Samanta, Sabyasachi Bandyopadhyay, and Abhishek Dey*

Department of Inorganic Chemistry, Indian Association for the Cultivation of Science, Kolkata, India 700032

S Supporting Information

ABSTRACT: Electrodes bearing thiolate and imidazole coordinated iron porphyrin catalysts are constructed and characterized using resonance Raman spectroscopy, absorption spectroscopy, and electrochemistry. The cyclic voltammetry data and their pH dependences are used to establish the nature of the exchangeable trans ligands in both of these cases. In situ monitoring of partially reduced oxygen species (PROS) produced during O₂ reduction using rotating ring disc electrochemistry (RRDE) experiments provide direct insight into the “push-effect” of the thiolate ligand. The thiolate bound iron porphyrin electrode generates highly oxidizing species on the electrode during electrocatalytic O₂ reductions which are very reactive. These surfaces can utilize these oxidants to catalytically hydroxylate strong C–H bonds using molecular O₂ with turnover numbers as high as 200.



1. INTRODUCTION

Metalloporphyrins are versatile catalysts for O₂ activation and reduction. In Hemoglobin (Hb) and Myoglobin (Mb) the heme active sites bind O₂ reversibly,^{1–3} in Cytochrome c Oxidases (CcO) O₂ is reduced to H₂O and in Cytochrome P450 the O₂ reduction is coupled to substrate oxidation.^{4–8} In fact, Cytochrome P450 efficiently activates very strong C–H bonds using molecular O₂ in nature.⁹ All these active sites have the same heme cofactor, but vary in coordinating axial ligands and distal environments. In Hb, Mb, and peroxidases the heme is ligated to the protein by an imidazole headgroup of a histidine residue (Figure 1A) while in Cytochrome P450 the heme is ligated by a thiolate headgroup of a cysteine residue (Figure 1B). The different proximal ligands are proposed to have different “push-effects”, and this has been a matter of great interest for some time now.¹⁰ In addition, different distal environments of some of these enzyme active sites are proposed to exert different “pull-effects”.¹⁰ Understanding the individual contributions of the different proximal ligands and distal environments to the diverse reactivities of these proteins have proved to be quite challenging. One of the key problems associated with the investigation of these effects in a protein active site by single point mutations of the active site residues is the possible change of protein conformation associated with it.

There is a growing demand for efficient man made catalysts that can catalyze the oxidation of inert C–H bonds using molecular O₂, a process that the Cytochrome P450 active site can catalyze efficiently under ambient conditions.^{11–13} In spite of great deal of research in this area, developing functional models of these active sites that reproduce these differences in axial and distal environments have been difficult using

conventional synthetic techniques. This is mainly due to complications associated with the synthesis of stable heme complexes with a thiolate axial ligand. Only a few are reported so far, and the ones reported are too unstable in the presence of O₂ or in aqueous solvent to perform any elaborate experiments to investigate these properties.^{14–16} There have been several reports of iron and manganese porphyrin complexes and some nonheme iron complexes that can catalyze substrate oxidation using peroxides, peracids, and iodosyl benzene.^{17–30} While there are several recent reports of stoichiometric hydroxylations of organic substrates using O₂ there are no reports of functional models or any catalyst that can catalytically oxidize C–H bonds using molecular O₂ like the native enzymes.^{31–36} In all known cases of C–H bond activation, a high-valent metal-oxo species is produced using oxygen atom transfer agents (peracids, peroxides), and this high-valent species activates inert C–H bonds. The challenge is to produce these species catalytically from molecular O₂.³⁷ For iron porphyrins this process generally requires both protons and electrons, for example, PFe^{II} + O₂ + 2H⁺ + e[–] → P⁺Fe^{IV}=O (compound I) + H₂O (where P represents a porphyrinato ligand). Homogeneous catalysis, however, has a very significant inherent limitation in this regard, that is, controlling simultaneous addition of both O₂ and electrons to the catalyst from the same homogeneous reaction medium. Rather, the oxidation of the reducing agent ($E^\circ = -200$ to -400 mV to reduce Fe-porphyrin) by either O₂ or H⁺ is facile. In nature such a situation does not arise because the source of electron (i.e., the reductase component) stays

Received: October 30, 2012

Published: January 28, 2013

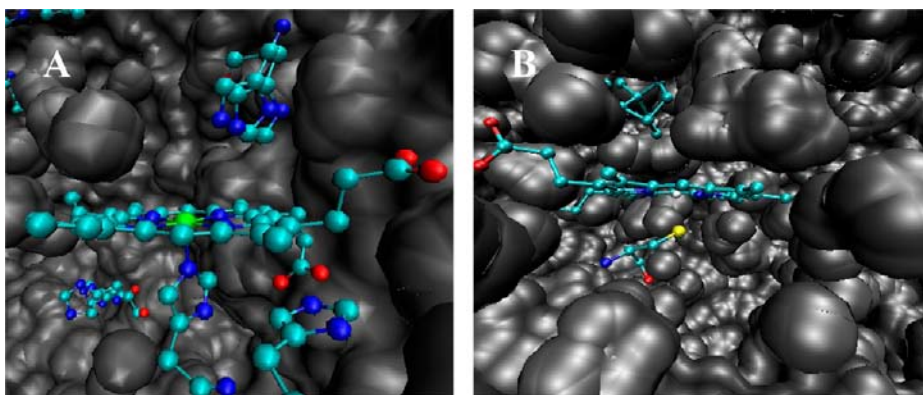
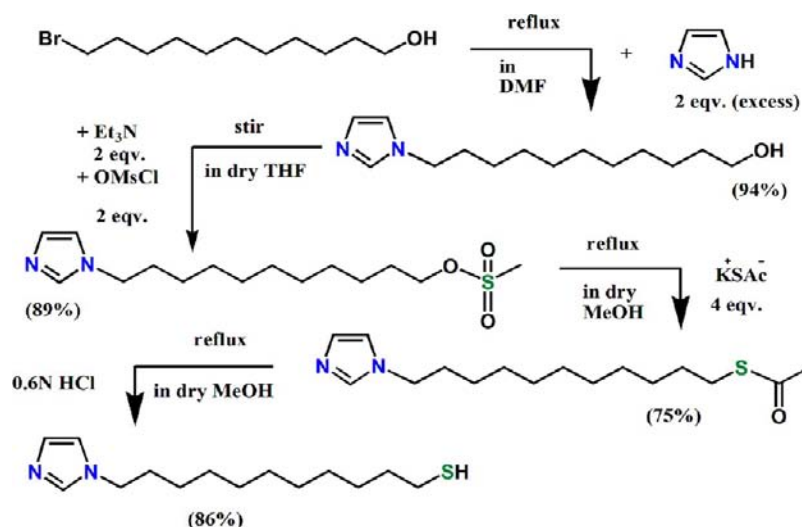


Figure 1. Active site structure of Myoglobin (A) (pdb id: 1A6M) and Cytochrome P450 (B) (pdb id: 1AKD).

Scheme 1. Schematic Presentation of the Synthesis of ImdC₁₁SH



protected in a protein active site and only transfers the electron to the active site. Further the electron transfer pathways and the H^+/O_2 transfer pathways leading into the enzyme active site are almost always orthogonal.

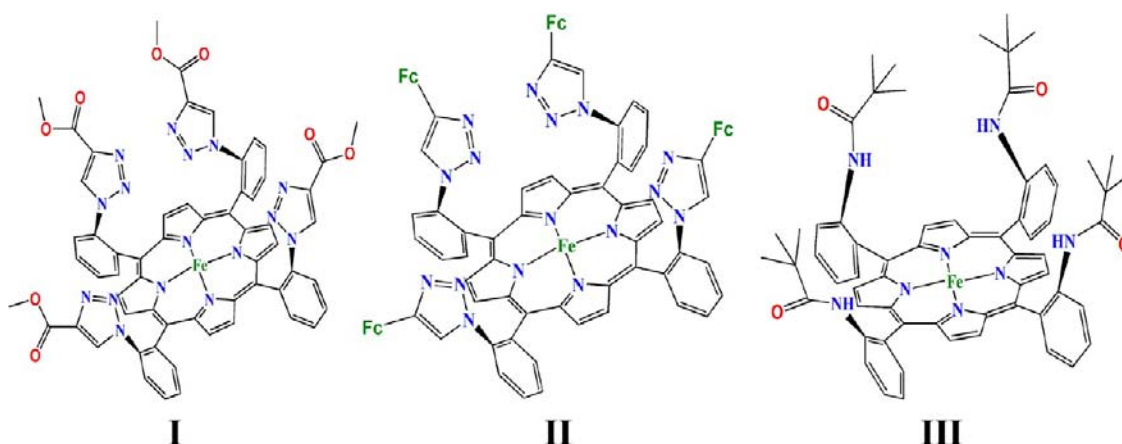
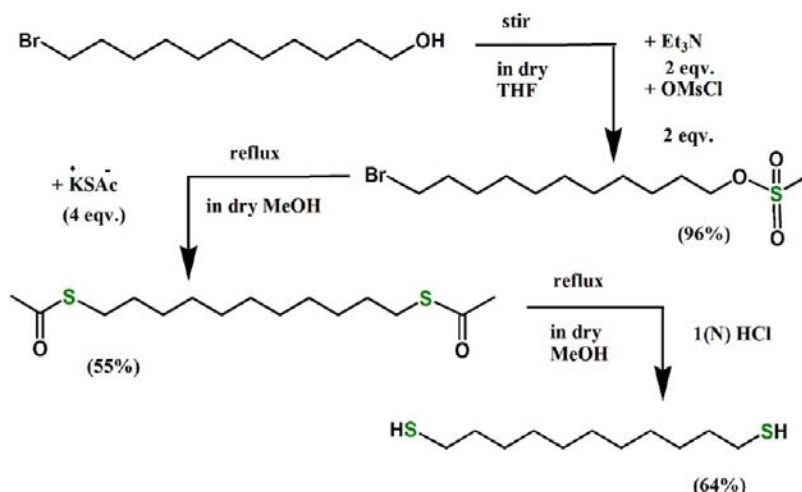
Self Assembled Monolayer (SAM) of thiols on Au and Ag electrodes have been widely used in chemistry and biology. These thiols can be further functionalized in several different ways to attach different types of molecules to these surfaces. These molecules range from small catalysts to DNA, proteins, antibodies, and viruses.^{38–45} There have been several reports where electrocatalysts have been covalently attached to SAM. In several reports “click chemistry” has been used as a method for these covalent attachments.^{46–48} Collman’s group reported the attachment of Ru porphyrin complexes on Au surfaces by simple covalent coordination.^{49,50} A similar method has recently been used by the Nemykin group where they have successfully attached Zinc Tetraferrocenyl porphyrins on alkyl thiol SAM bearing an imidazole headgroup.⁵¹ This strategy can be used to construct a surface where the catalysts, bound to terminal functional headgroups, can be thinly dispersed between aliphatic thiols (referred to as diluents) thus allowing formation of site isolated active sites. The thiols insulate the electrode, source of electrons, from the bulk solution, source of H^+ and O_2 . Electrons are transferred to the catalytic center from the electrode via covalent bonds (C–C bonds). This mimics the inherent heterogeneity of protein active sites

discussed above. Further the rate of electron transfer from the electrode to the catalyst can be controlled by using thiols of varying chain lengths.

In this paper we report the formation of bioinspired catalytic surfaces which have been constructed, characterized, and used for catalyzing vital multielectron and multiproton reactions, in particular, O_2 activation. Linkers, having a thiol group at one end, and a coordinating residue (imidazole/thiol) on the other terminal were synthesized. SAM functionalized Au electrodes having these different linkers which behave as different axial ligands were constructed. Various site isolated iron porphyrin based active sites differing in distal environment have been assembled on these surfaces by simple reversible covalent attachment. The surfaces were characterized by electrochemical and spectroscopic methods. These modified electrodes can catalytically oxidize cyclohexane and toluene using molecular O_2 .

2. EXPERIMENTAL DETAILS

2.1. Materials. All reagents were of the highest grade commercially available and were used without further purification. 11-Bromo undecan-1-ol (BrC₁₁OH), Methane sulfonyl chloride (OMsCl), Potassium thioacetate (KSAc), Octanethiol (C₈SH), potassium hexafluorophosphate (KPF₆), cyclohexanone, benzylalcohol, and all buffers were purchased from Sigma-Aldrich. Disodium hydrogen phosphate dihydrate (Na₂HPO₄·2H₂O), potassium chloride (KCl), imidazole (Imd), conc. Hydrochloric acid (HCl), cyclohexane, and

Scheme 2. Schematic Presentation of the Synthesis of SHC₁₁SHFigure 2. Pictorial representation of the catalysts used. (I) FeEs₄, (II) FeFc₄, and (III) Fe “picket-fence”.

cyclohexanol were purchased from Merck. Triethylamine (Et₃N), *p*-cresol, and toluene were purchased from Spectrochem India Ltd. Au wafers were purchased from Platypus Technologies (1000 Å of Au on 50 Å of Ti adhesion layer on top of a Si(III) surface). Transparent Au wafers (100 Å of Au on 10 Å of Ti) were purchased from Phasis, Switzerland. Au discs for the Rotating Ring Disc Electrochemistry (RRDE) experiments and Ag discs for Surface Enhanced Resonance Raman Spectroscopy (SERRS) experiments were purchased from Pine Instruments, U.S.A.

2.2. Instrumentation. UV–vis absorption data were taken in an Agilent technologies spectrophotometer model 8453 fitted with a diode-array detector. All electrochemical experiments were performed using a CH Instruments (model CHI710D Electrochemical Analyzer). Biopotentiostat, reference electrodes, Teflon plate material evaluating cell (ALS Japan) were purchased from CH Instruments. The RRDE set up from Pine Research Instrumentation (E6 series ChangeDisk tips with AFE6M rotor) was used to obtain the RRDE data. Surface Enhanced Resonance Raman data were collected using a Trivista 555 spectrograph (Princeton Instruments) and using 413.1 nm excitation from a Kr⁺ laser (Coherent, Sabre Innova SBRC-DBW-K). The FT-IR data were measured on a Shimadzu FT-IR 8400S instrument. All the NMR spectra were recorded on a Bruker DPX-300 or DPX-500 spectrometer at room temperature. The mass spectra were recorded by QTOF Micro YA263 instrument. Gas Chromatography (GC) measurements were carried in an Agilent 6890N Network GC system.

2.3. Synthesis. **2.3.1. 11-Imidazolyl Undecan-1-thiol (ImdC₁₁SH).** The desired product was obtained starting from 11-Bromo undecan-1-ol through a series of steps as shown in Scheme 1. 11-Bromo undecan-1-ol was refluxed with excess imidazole in DMF

followed by stirring with OMsCl and Et₃N which substituted –OH by the mesyl group. The mesyl group was substituted by thioacetate group followed by refluxing in 0.6 (N) HCl to obtain the thiol group.

2.3.2. Undecan-1,11-dithiol (SHC₁₁SH). The desired product was obtained starting from 11-Bromo undecan-1-ol through a series of steps as shown in Scheme 2. 11-Bromo undecan-1-ol was stirred with OMsCl and Et₃N in dry tetrahydrofuran (THF) to substitute –OH by the mesyl group. The mesyl and bromo groups were substituted by the thioacetate group by refluxing with 4 equiv of KSAc in dry MeOH followed by refluxing in 1 (N) HCl to obtain the dithiol product.

2.3.3. Picket-fence Iron(II) Porphyrin (Fe “picket-fence”), α₄-Tetra-2-(4-ferrocenyl-1,2,3-triazolyl)-phenylporphyrinato Iron (FeFc₄) and α₄-Tetra-2-(4-carboxymethyl-1,2,3-triazolyl)-phenylporphyrinato Iron (FeEs₄). The catalysts have been prepared in our laboratory. Fe “picket-fence” has been synthesized as reported.⁵² The detailed synthetic scheme of the other two clickable porphyrins has been reported elsewhere.^{53,54} The catalysts have been pictorially presented in Figure 2.

2.4. Construction of the Electrodes. **2.4.1. Formation of Mixed SAM.** Au wafers and discs were cleaned electrochemically by sweeping several times between 1.5 V to –0.3 V in 0.5 M H₂SO₄. Ag discs were cleaned in alumina (size: 1 μ, 0.3 μ, and 0.05 μ) and then roughened in 0.1 M KCl solution as described in literature. SAM solutions were prepared using the concentration ratio of the linkers as shown in Table 1. In each case the diluent used was C₆S₆H₆. Freshly cleaned Au wafers and discs and freshly roughened Ag discs were rinsed with triple distilled water, ethanol, purged with N₂ gas, and immersed in the depositing solution for 48 h. Freshly cut transparent Au wafers, used in

Table 1. SAM Solution Preparation Ratios^a

linkers	mole-fraction	total concentration
ImdC ₁₁ SH	0.2	0.4 mM
SHC ₁₁ SH	0.2	3 mM ⁵⁵

^aC₈SH was used as diluent.

absorption spectroscopy, were washed with ethanol, dried with N₂ gas, and immersed in the SAM solution for the same period of time.

2.4.2. Attachment of the Catalysts on to the SAM. Au wafers and discs and roughened Ag discs immersed in the deposition solution were taken out before experiments and rinsed with ethanol followed by triple distilled deionized water and then dried with N₂ gas. The wafers were then inserted into a Plate Material Evaluating Cell (ALS Japan), and the discs were mounted on a platinum ring disc assembly (Pine Instruments, U.S.A.). Solutions of the catalysts were prepared in chloroform. For the attachment of the Fe “picket-fence” to the ImdC₁₁SH linker the electrode surface was immersed in CHCl₃ solution of the catalyst for about 1.5 h. For the SHC₁₁SH linker the electrode surfaces were immersed first in Et₃N for 10 min and then in the Fe “picket-fence” porphyrin solution for 2.5 h (Scheme 3). For the attachment of FeFc₄ and FeEs₄ catalysts to the ImdC₁₁SH linker the electrode surface was immersed in the catalyst solution for about 1 h, and for the SHC₁₁SH linker the surfaces were immersed in a solution of Et₃N and catalyst for 1.5 h. After the respective times the surfaces were thoroughly rinsed with chloroform, ethanol, and triple distilled water before the electrochemical or SERRS experiments.

2.4.3. Physiabsorption vs Covalent Attachment. Iron porphyrins are known to physiabsorb on thiol surfaces. However, the work of Collman and Chidsey has shown that thorough rinsing of the surface with an organic solvent like CH₂Cl₂ or CHCl₃ removes any physiadsorbed material.⁴⁷ Control experiments were performed where the electrocatalytic behavior of these surfaces were monitored before and after washing with CHCl₃. The data clearly show that the physiadsorbed complexes, which remain on the surface before washing with CHCl₃, show O₂ reduction at very different potentials (Figure S1 and S2, Supporting Information). However these species are easily removed on washing with CHCl₃ (Figure S3, Supporting Information).

2.5. Absorption Spectroscopy. For the heterogeneous absorption experiment, covalently attached catalysts on SAM modified transparent Au electrodes were used.

2.6. Cyclic Voltammetry (CV) Experiments. All CV experiments were done in pH 7 buffer (unless otherwise mentioned) containing 100 mM Na₂HPO₄·2H₂O and 100 mM KPF₆ (supporting electrolyte) using Pt wire as the counter electrode and Ag/AgCl as the reference electrode.

2.7. Coverage Calculation. The coverage for a particular species was estimated by integrating the oxidation and reduction currents of the respective species.^{47,56} In parallel the porphyrin attached to SAM (on a 2 cm² wafer) was extracted into CH₂Cl₂ solvent by protonation

of the thiol/imidazole using CF₃COOH. The absorbance of the resultant solution (reduced to 100 μL) is 0.005 units. Assuming an ϵ of 10⁵ M⁻¹ s⁻¹, this yields a concentration of 5 × 10⁻⁷ M, that is, 7 × 10⁻¹¹ moles of porphyrin are present in 2 cm² of the wafer. So the coverage is 3.5 × 10⁻¹¹ mol/cm². This is consistent with the estimate obtained under the integrated charge of the CV waves.

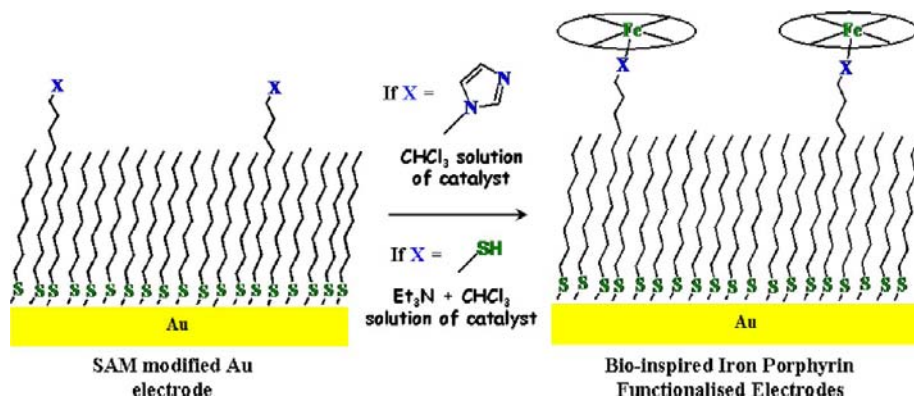
2.8. Partially Reduced Oxygen Species (PROS). The Pt ring and the Au disc were both polished by alumina powder (grit sizes: 1 μm, 0.3 μm, and 0.05 μm) and electrochemically cleaned and inserted into the RRDE tip (Figure 3A) which was then mounted on the rotor and immersed into a cylindrical glass cell equipped with Ag/AgCl reference and Pt counter electrodes. The collection efficiency (CE) of the RRDE setup was measured in a 2 mM K₃Fe(CN)₆ and 0.1 M KNO₃ solution at 10 mV/S scan rate and 300 rpm rotation speed. A 20 ± 2% CE was generally recorded during these experiments (Figure 3B). The potential at which the ring was held during the collection experiments at pH 7 for detecting H₂O₂ was obtained from literature.⁵⁷

2.9. Surface Enhanced Resonance Raman Spectroscopy (SERRS). Ag discs were cleaned using Alumina powder (grit sizes 1, 0.3, and 0.05 μm) and then roughened in a 0.1 M KCl solution using reported procedures^{58,59} and immersed in SAM solutions. The roughened modified Ag discs were then inserted into the RRDE setup for the collection of SERRS data.^{60,61} Catalysts were attached in a similar manner as described in section 2.4.2. Experiments were done using an excitation wavelength of 413.1 nm, and the power used at the electrode surface was around 10–12 mW.

2.10. Substrate Oxidation. Substrates used here were toluene and cyclohexane. Buffer solutions (pH 7) were saturated with the substrate by vigorously shaking a suspension of these organic molecules in water. The mixture was allowed to settle and separated using a separating flask. The aqueous layer was extracted and O₂ reduction CV experiments were performed on the surfaces (3 Linear Sweep Voltammetry between 0.5 V to -0.5 V). The resultant aqueous solutions were extracted with Chloroform (CHCl₃). The CHCl₃ layer was evaporated, and the product left behind was subjected to ESI-MS and GC and GC-MS analysis.

2.11. Estimation of Turnover Number (TON). The amount of product was quantified using GC against known concentrations of pure compounds. As a control the same process, outlined above, was followed but without performing the electrochemical O₂ reductions in these solution. In such cases no new products were detected in the GC. The CV experiments were used to calculate the number of catalysts on the surface (Section 2.7). The ratio of the number of moles of product formed and the number of moles of catalyst present yields the turnover number. Further, the integration of the O₂ reduction current provides the moles of O₂ reduced. The ratio of the moles of substrate oxidized (obtained from GC) and the moles of O₂ reduced is the Faradaic yield (FY) of the process. Typically FY of 9–10% was recorded, that is, only 9–10% of the reactive intermediates produced oxidized the substrate.

Scheme 3. Schematic Representation of Construction of the Bio-Inspired Electrodes



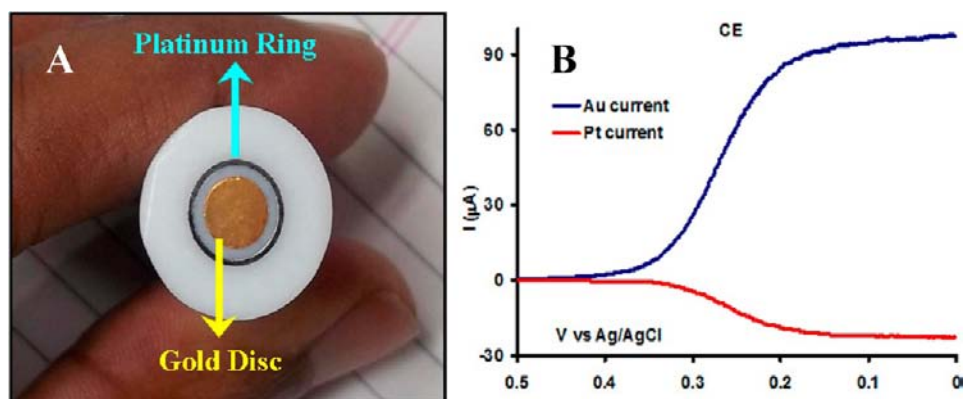


Figure 3. (A) RRDE assembly showing the Au disc and Pt ring. (B) A Collection efficiency plot.

3. RESULTS AND ANALYSIS

3.1. Absorption Spectroscopy. Iron porphyrins have an intense Soret band which helps in monitoring these complexes after attachment on the modified surfaces. Absorption data obtained on FeFc₄ attached to the imidazole linker show a Soret at 422 nm (Figure 4A, red). When the sample is reduced by dithionite solution the Soret shifts to 432 nm (Figure 4A, green), which upon binding CO sharpens and moves to 426 nm (Figure 4A, blue).⁶² These values are consistent with

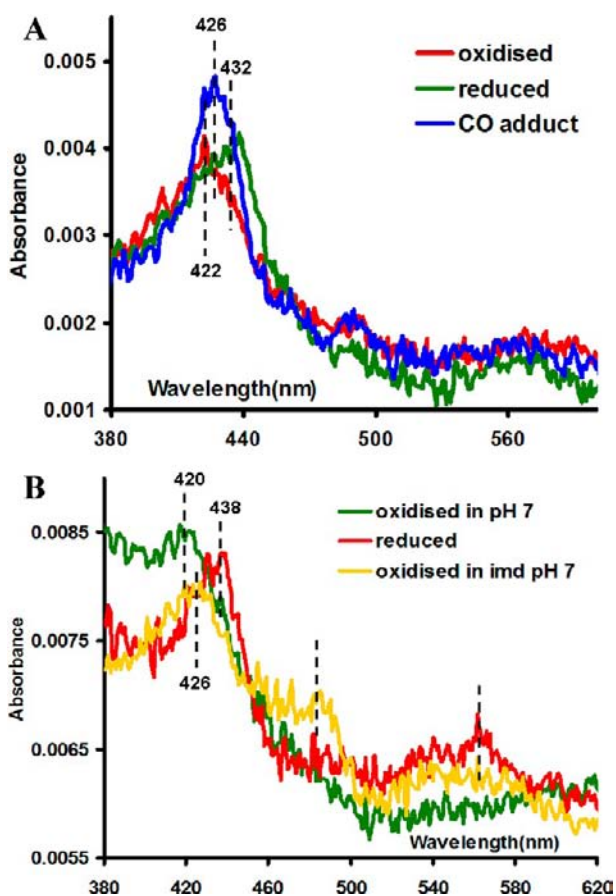


Figure 4. (A) Absorption spectra of FeFc₄ attached to a monolayer of ImdC₁₁SH when oxidized (red), reduced (green), and when reduced and CO bound (blue) in pH 7. (B) Similar spectra of FeFc₄ attached to SHC₁₁SH when oxidized (green), reduced (red) in pH 7 and in 100 mM imidazole containing pH 7 (yellow).

previous reports of imidazole coordinated Fe-porphyrin.⁶³ Absorption data obtained on electrode bearing the FeFc₄ attached to dithiol linker show a Soret at 420 nm (Figure 4B, green) which upon reduction shifts to 438 nm. Upon reduction a 565 nm band at the Q-band region is also seen. Binding CO to the reduced complexes results in a Soret at 422 nm and not at 450 nm as may be expected for a P450 like active site (Figure S4, Supporting Information). These results reproduce previous reports on several thiolate bound heme active sites and is likely due to protonation of the thiolate ligand on CO binding.⁶⁴ When the catalyst is bound to imidazole the Soret shifts from 420 to 426 nm indicating the formation of a low spin (LS) complex upon binding strong donor like imidazole (Figure 4B, yellow).^{65,66} A band at 482 nm gains intensity when bound to the external imidazole ligand. The origin of this band is uncertain at this point. These absorption data may not be directly correlated to the data reported for protein active sites in solution as coupling of the surface plasmons is known to alter the electronic structure of thiolate bound heme active sites.⁶⁷ The observed values and their changes with changes in oxidation state of iron and the trans axial ligand (e.g., H₂O, CO, imidazole) are in general consistent with previous reports on P450 and thiolate bound heme complexes. These data are collected on a monolayer modified transparent electrode surface and thus appear noisy if compared to solution and in many cases the value of the Soret transition can only be tentatively assigned. However, in spite of such dilution, the very high absorption coefficient of the porphyrin results in reasonable absorption features.^{68,69,51} Considering the molar extinction coefficient of native P450 ($\sim 10^5 \text{ M}^{-1} \text{ cm}^{-1}$), the beam area (0.385 cm²), and the path-length (0.1 cm) of the cell, the number of molecules (i.e., the coverage) has been estimated to be around $1.5 \pm 0.5 \times 10^{-11} \text{ mol/cm}^2$. In parallel, the porphyrin attached to the SAM was extracted in a CH₂Cl₂ solution. The concentration of the porphyrin in the solution is estimated using UV-vis absorption spectroscopy, and the coverage thus estimated is $\sim 3.5 \times 10^{-11} \text{ mol/cm}^2$.

3.2. Surface Enhanced Resonance Raman Spectroscopy (SERRS). The SERRS spectra of the FeEs₄ complex attached to the imidazole linker show the oxidation and spin state marker ν_4 and ν_2 bands at 1367 cm⁻¹ and 1566 cm⁻¹, respectively (Figure 5A, orange). This reflects a LS ferric state of the Iron. The corresponding ν_4 vibrations for the thiolate linker is at 1365 cm⁻¹, and there are two ν_2 vibrations at 1551 cm⁻¹ and 1565 cm⁻¹ indicating that there is a mixture of high spin (HS) (ν_2 at 1551 cm⁻¹) and LS (ν_2 at 1565 cm⁻¹) species (Figure 5A, blue).^{70,71} The ν_8 vibration which represents the

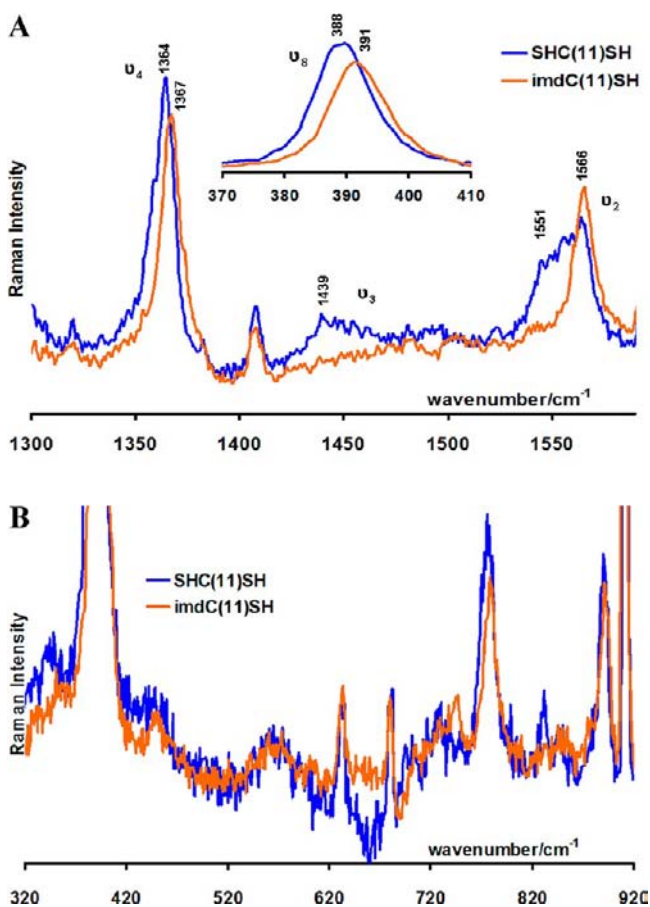


Figure 5. SERRS data of FeEs_4 when attached to $\text{ImdC}_{11}\text{SH}$ (orange) and SHC_{11}SH (blue) in the (A) high frequency region and in the (B) low frequency region.

symmetric $\text{Fe}-\text{N}_{\text{pyrrole}}$ stretch, is at 391 cm^{-1} for the imidazole linker, and it shifts to 388 cm^{-1} for the thiolate linker (Figure 5A, inset) consistent with previous results.⁷² This may reflect the stronger donation by the anionic covalent thiolate donor which weakens the $\text{Fe}-\text{N}_{\text{pyrrole}}$ bond. However, this comparison is only speculative as the ν_8 of the thiolate bound site is a mixture of HS and LS species.

In the low frequency region, additional vibrations are observed for the thiolate linker at 341 cm^{-1} and 675 cm^{-1} (Figure 5B). Further there is an increase in intensity of the 770 cm^{-1} vibration. It is tempting to assign the 341 cm^{-1} vibration as a $\text{Fe}-\text{S}$ stretching mode for the HS species⁷³ and the 675 cm^{-1} vibration and the 770 cm^{-1} vibration as $\text{C}-\text{S}$ stretching modes. However, such assignment needs appropriate isotopic substitution to be confirmed which is beyond the scope of this study.

In the presence of 100 mM imidazole, the SERRS data of the FeEs_4 complex attached to the thiolate linker show the ν_4 and ν_2 vibrations at 1366 cm^{-1} and at 1565 cm^{-1} indicating that a LS species exists under these conditions (Supporting Information, Figure S5, gray).⁷¹ Thus binding of an external axial imidazole ligand increases the population of LS species on these surfaces, consistent with the data obtained with imidazole linker.

The SERRS data of FeFc_4 bound to imidazole SAM (Figure 6A, blue) show the ν_4 and the ν_2 bands at 1368 cm^{-1} and 1566 cm^{-1} , respectively, indicating that the Fe in the complex is in a LS Fe(III) state. Alternatively, the SERRS data of the FeFc_4

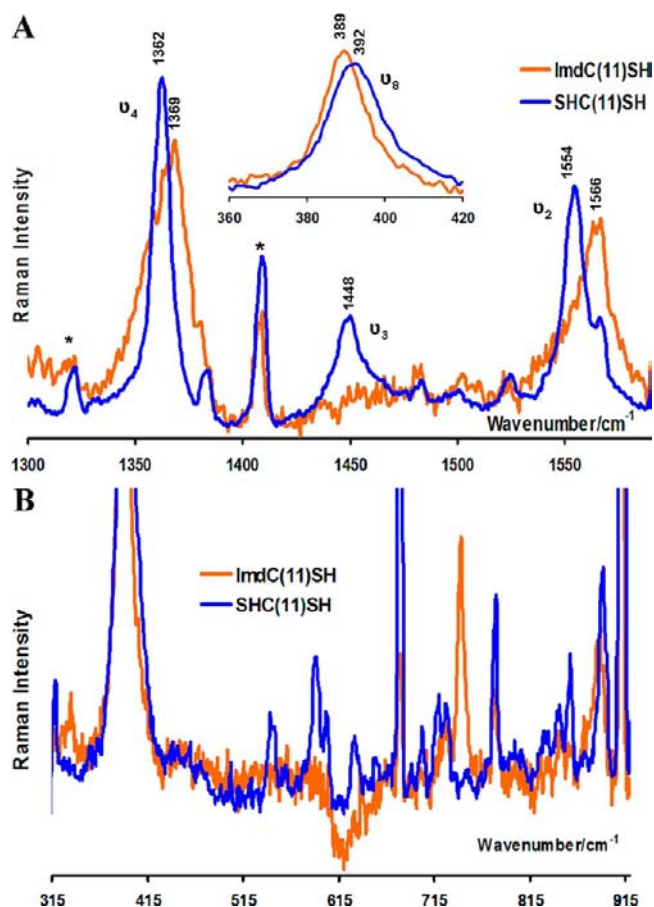


Figure 6. SERRS data of FeFc_4 when attached to $\text{ImdC}_{11}\text{SH}$ (blue) and SHC_{11}SH (orange) in the (A) high frequency region and in the (B) low frequency region.

complex bound to the dithiol SAM (Figure 6A, orange) show a major species with the ν_4 , ν_3 , and ν_2 bands at 1363 cm^{-1} , 1448 cm^{-1} , and 1556 cm^{-1} , respectively. This originates from a HS Fe(III) center. The ν_2 region shows a shoulder at 1567 cm^{-1} indicating the presence of a minor LS Fe(III) species. Overall these results are consistent with those observed for the FeEs_4 complex, that is, the imidazole bound complex is mainly LS while the thiolate bound complex is a mixture of high and LS species. In the low frequency region, unique vibrations are observed between 520 cm^{-1} and 741 cm^{-1} (Figure 6B, blue). These vibrations may originate from the $\text{Fe}-\text{S}-\text{C}$ motif ($\text{C}-\text{S}$ stretching vibration) and can only be assigned with appropriate isotopic substitution.

In the presence of 100 mM imidazole, the SERRS data of the FeFc_4 complex attached to the thiolate linker is similar to that of the FeEs_4 complex. The ν_4 and ν_2 vibrations appear at 1369 cm^{-1} and at 1566 cm^{-1} , respectively, indicating that the iron porphyrin complex exists as a purely LS species (Supporting Information, Figure S6, gray) on binding an axial imidazole ligand.

SERRS data of Fe “picket-fence” complex attached to the imidazole SAM (Figure 7, blue) show the ν_4 and the ν_2 bands at 1364 cm^{-1} and 1554 cm^{-1} , respectively, indicating that the Fe in the complex is in a HS Fe(III) state.⁷¹ For the thiolate bound Fe “picket-fence” catalyst the ν_4 band appears at 1362 cm^{-1} and the ν_2 band appears at 1554 cm^{-1} and 1566 cm^{-1} indicating the presence of the Fe in the complex as a mixture of HS and LS Fe(III) states (Figure 7, orange). In the presence of

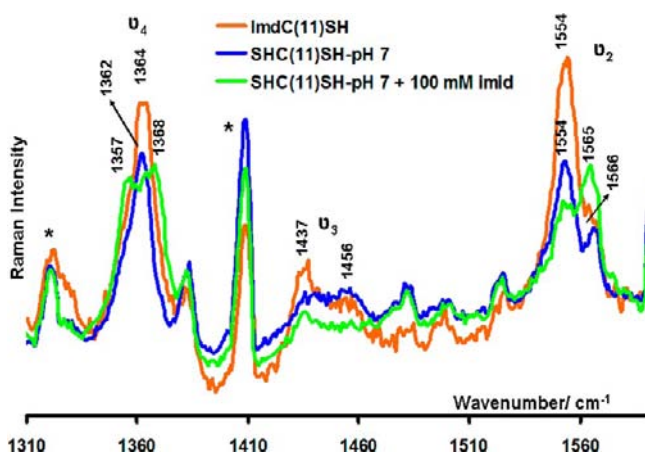


Figure 7. SERRS data of the Fe “picket-fence” attached to ImdC₁₁SH (blue) and SHC₁₁SH in pH 7 (orange) and 100 mM imidazole containing pH 7 (green).

100 mM imidazole, the SERRS data of the Fe “picket-fence” complex attached to the thiolate linker show the increase in LS Fe(III) state (Figure 7, green).

The SERRS data obtained for the different catalysts are summarized in Table 2. The data suggest clear differences in the SERRS data of these catalysts bound to linkers and the data obtained by physisorbing these catalysts on octane thiol surfaces. In particular for the physisorbed surfaces the ν_3 vibration is $>1450\text{ cm}^{-1}$, the ν_4 and the ν_2 vibrations and the distribution of the HS and LS species are quite distinct from those obtained for the coordinated surfaces (Supporting Information, Figure S7, and Table 2). Further the spin states of the iron center depend on the nature of the coordinating ligand. The triazole bearing porphyrins stabilize a LS ground state with an imidazole ligand but result in a dominantly HS state (minor LS species present as well) with a thiolate ligand. Note that this distribution of HS and LS is also seen for the P450 enzyme and its mutant.^{74,75} In addition to these there are several unique vibrations in the low energy region of the SERRS spectra which agree with known values of Fe–S and C–S vibrations supporting the formation of thiolate coordinated heme sites on the surface. The Fe “picket-fence” complex bound to the imidazole is HS. However, all of these complexes become LS when incubated in a 100 mM imidazole buffer due to an exogenous imidazole binding. Unfortunately SERRS data could not be obtained on the FeFc₄ and the FeEs₄ bound to the imidazole linker in the presence of 100 mM imidazole as it led

to dissociation of the iron porphyrin from the surface (vide infra).

3.3. Electrochemistry. The CV of the Fe “picket-fence” complex functionalized electrodes show a well developed Fe^{III}/Fe^{II} CV for both imidazole and thiolate linkers in the absence of O₂ (Figure 8). For the imidazole linker the $E_{1/2}$ of the

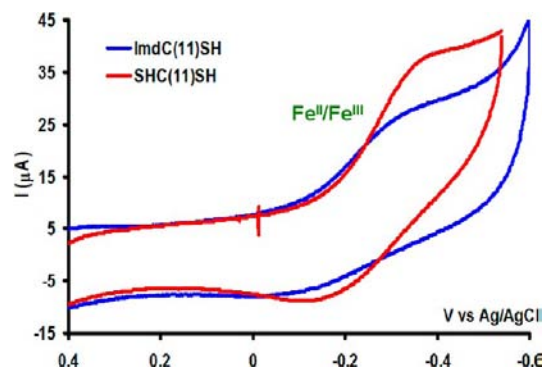


Figure 8. CV data of Fe “picket-fence” in deoxygenated pH 7 buffer when attached to ImdC₁₁SH (blue) and SHC₁₁SH (red) using Ag/AgCl as reference and Pt wire as counter electrodes under Ar atmosphere.

porphyrin Fe^{III}/Fe^{II} process is at -217 mV (Figure 8, blue) and for the thiolate linker this value is obtained at -250 mV (Figure 8, red, Table 3). Note that the reduction of the iron could lead

Table 3. Observed $E_{1/2}$ Values (mV)

catalyst	ImdC ₁₁ SH	SHC ₁₁ SH
Fe “picket-fence”	-217	-250
FeFc ₄	Fc ⁺ /Fc	365
	Fe ^{III} /Fe ^{II}	-210
		-244

to ligand dissociation. However that would lead to loss of catalyst from the surface and there will be loss of CV intensity between successive scans. However that is not the case indicating that both the oxidized and reduced iron porphyrin complexes are bound to the surface.

Similarly, the CV of the FeFc₄ catalyst functionalized electrodes show well developed Fc⁺/Fc and Fe^{III}/Fe^{II} CVs for both imidazole and thiolate linkers in the absence of O₂ (Figure 9). For the imidazole linker the $E_{1/2}$ of the Fc⁺/Fc and the porphyrin Fe^{III}/Fe^{II} processes are at 365 mV and -210 mV , respectively (Figure 9, blue). For the thiolate linker these values are obtained at 362 mV and -244 mV , respectively (Figure 9,

Table 2. Marker Bands (in cm^{-1}) of Different Fe-Porphyrins Attached to SHC₁₁SH or ImdC₁₁SH Linker in pH 7 Buffer

linker		ν_4	ν_3	ν_2	ν_8
FeEs ₄	C ₈ SH	1363	1450	1557/1564	388
	SHC ₁₁ SH	1364	1439	1551/1565	388
	SHC ₁₁ SH (with 100 mM imidazole)	1366		1565	389
	ImdC ₁₁ SH	1367		1566	391
FeFc ₄	C ₈ SH	1362/1367	1454	1555/1565	390
	SHC ₁₁ SH	1363	1448	1556/1567	392
	SHC ₁₁ SH (with 100 mM imidazole)	1369		1566	391
	ImdC ₁₁ SH	1369		1566	389
Fe “picket-fence”	SHC ₁₁ SH	1362	1438/1456	1554/1566	392
	SHC ₁₁ SH (with 100 mM imidazole)	1357/1368		1554/1565	393
	ImdC ₁₁ SH	1364	1437/1454	1554	396

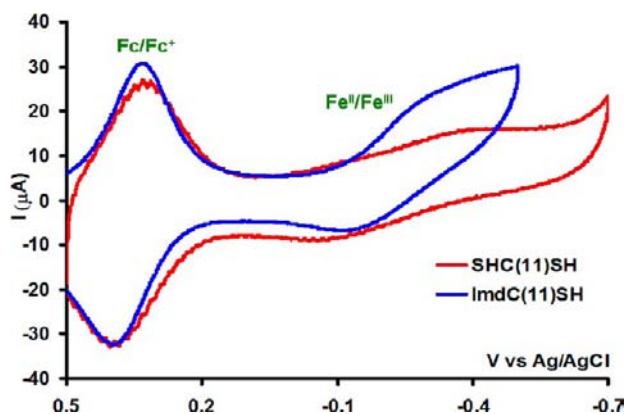


Figure 9. CV data of FeFc_4 in deoxygenated pH 7 buffer when attached to $\text{ImdC}_{11}\text{SH}$ (blue) and SHC_{11}SH (red) using Ag/AgCl as reference and Pt wire as counter electrodes under Ar atmosphere.

red, Table 3). In the presence of CO when FeFc_4 is bound to thiolate the Fc/Fc^+ CV appears at same potential but the $\text{Fe}^{\text{III}}/\text{Fe}^{\text{II}}$ CV is not observed consistent with thiolate protonation indicated by the UV-vis data (Figure S8, Supporting Information). The electroactive ferrocene group acts as an internal redox marker, and it does not shift depending on the linker. Thus, for both the Fe “picket-fence” and FeFc_4 catalysts, the $\text{Fe}^{\text{III}/\text{II}}$ process shifts to negative potentials for the thiolate linker relative to the imidazole linker. The CV data for the $\text{Fe}^{\text{III}/\text{II}}$ couple is much broader than that of the Fc^+/Fc couple. This may be because of the presence of two different spin states of these complexes (see SERRS data above) resulting in two different redox processes under the same wave.⁷⁶

The integration of the current under the Fc^+/Fc and/or $\text{Fe}^{\text{III}/\text{II}}$ processes yields the total number of electroactive species immobilized on the surface, that is, surface coverage (Table 4).⁴⁷ The Fe “picket-fence” shows coverage of 0.7% and 0.9%

Table 4. Calculated Surface Coverages (%)

catalyst		$\text{ImdC}_{11}\text{SH}$	SHC_{11}SH
Fe “picket-fence”		0.9 ± 0.02	0.7 ± 0.05
FeFc_4	Fc^+/Fc	6.6 ± 0.03	6.6 ± 0.03
	$\text{Fe}^{\text{III}}/\text{Fe}^{\text{II}}$	1.6 ± 0.05	1.4 ± 0.05

on thiol and imidazole functionalized SAM, respectively. For the FeFc_4 complex the coverages for the Fc^+/Fc and $\text{Fe}^{\text{III}/\text{II}}$ processes are found to be 6.6% and 1.4% and 6.6% and 1.6% on thiol and imidazole functionalized SAM, respectively. Thus the Fc^+/Fc current is about four times that of $\text{Fe}^{\text{III}/\text{II}}$, consistent with the stoichiometry of the molecule (i.e., four Fc groups per Fe heme center). Note that $\sim 1\%$ coverage of the total electroactive surface indicates that a very dilute monolayer of catalyst is present on the electrode.⁷⁷

CV experiments are performed at different pHs to gain insight into the nature of trans axial ligand. For the imidazole linker, both Fe “picket-fence” and FeFc_4 complexes show a pH dependent $E_{1/2}$ process (Figure 10A and 10B, blue). Note that Fc^+/Fc process in the FeFc_4 complex is pH independent. The $E_{1/2}$ for the porphyrin bound $\text{Fe}^{\text{III}/\text{II}}$ shifts to more negative values at higher pHs. Approximately 60 mV shift in $E_{1/2}$ per unit shift in pH is observed between pH 6–8 characteristic of a single proton coupled electron transfer (PCET) process and is consistent with an $\text{Imd-Fe}^{\text{III}}\text{-OH} + \text{e}^- + \text{H}^+ = \text{Imd-Fe}^{\text{II}}\text{-OH}_2$ redox equilibrium.^{78,79} The data also suggest that the pK_a 's

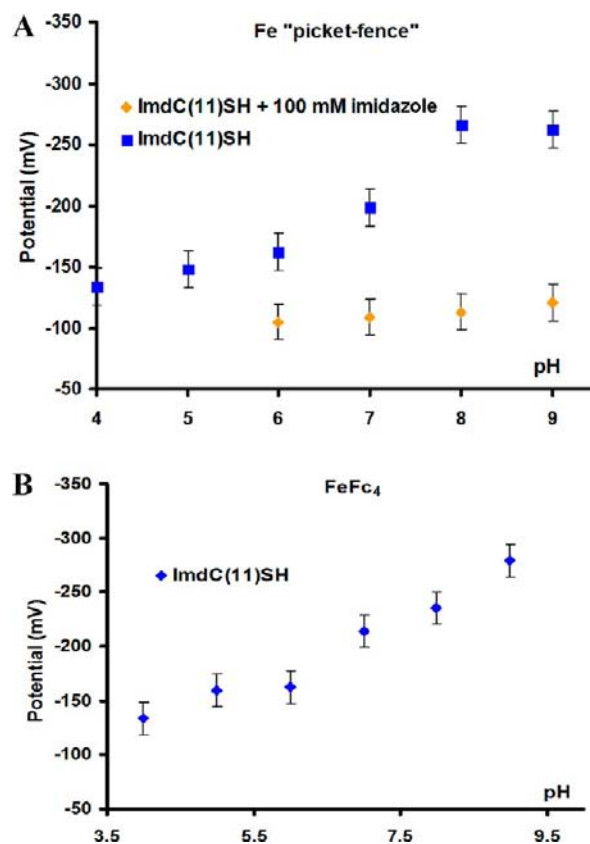


Figure 10. Plot of $E_{1/2}$ values at various pHs of Fe “picket-fence” (A) and FeFc_4 (B) attached to $\text{ImdC}_{11}\text{SH}$ SAM vs pH with (orange) and without (blue) 100 mM imidazole.

involved are higher for the FeFc_4 complex relative to the Fe “picket-fence” complex.⁸⁰ In the presence of 100 mM imidazole in the buffer, the pH dependence of the $\text{Fe}^{\text{III}/\text{II}}$ process for the “picket-fence” complex is abolished.⁸¹ This is consistent with the replacement of the ionizable H_2O ligand by non-ionizable imidazole, that is, $\text{Imd-Fe}^{\text{III}}\text{-Imd} + \text{e}^- = \text{Imd-Fe}^{\text{II}}\text{-Imd}$. The original electrochemistry behavior is reinstated once the imidazole containing buffer is replaced with normal pH 7 buffer.

In the case of thiolate linker, the CV data of the FeFc_4 and the Fe “picket-fence” complexes indicate that the $E_{1/2}$ shows little pH dependence between pHs 6–9 (Figure 11A and 11B) relative to the imidazole linker. This is consistent with a $\text{RS-Fe}^{\text{III}}\text{-OH}_2 + \text{e}^- = \text{RS-Fe}^{\text{II}}\text{-OH}_2$ redox equilibrium. SERRS data indicate that the thiolate linker results in a mixture of HS and LS species (vide supra). However, the pH dependence of $E_{1/2}$ indicate that in both of these cases (i.e., HS and LS) a PCET is not involved.

In summary, the pH dependent CV data suggest that these complexes bear a trans OH^- ligand when bound to imidazole and a trans H_2O ligand when bound to thiolate at pH 7. In the case of the imidazole linker, the trans OH^- ligand is protonated upon reduction and hence its $E_{1/2}$ follows a pH dependence befitting a PCET mechanism.⁷⁹ Alternatively, no protonation is involved in the case of the thiolate linker, and hence its $E_{1/2}$ is pH independent.

3.4. O_2 Reactivity. **3.4.1. O_2 Reduction.** In the presence of O_2 in the buffer a linear sweep voltammetry (LSV) experiment shows large electrocatalytic O_2 reduction currents at negative potentials for all the three catalysts for both imidazole and

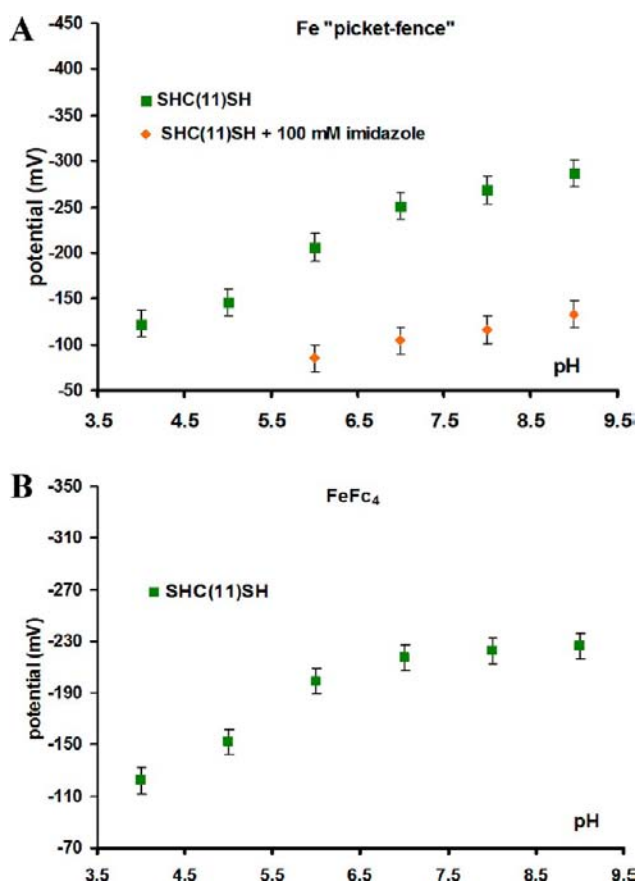


Figure 11. Plot of $E_{1/2}$ values at various pHs of Fe "picket-fence" (A) and FeFc₄ (B) attached to SHC₁₁SH SAM vs pH with (orange) and without (green) 100 mM imidazole.

thiolate linkers (Figure 12). Note that at these potentials the iron porphyrin catalyst is reduced to Fe^{II} (Figure 8 and 9). The data indicate that for the thiolate linker the O₂ reduction occurs at more negative potentials relative to an imidazole linker (Figure 12).^{82–84} This is consistent with lower reduction potentials of the thiolate ligated complexes and reflects that when bound to an anionic thiolate linker more driving force is needed to reduce O₂ relative to a neutral imidazole linker. The potentials for O₂ reduction where no linker is present (i.e., catalyst physisorbed on thiol surfaces) are distinct from these potentials (Section 2.4.3). This, in addition to the SERRS and UV–vis data, clearly indicates the formation of thiolate and imidazole coordinated active sites on the electrode.

3.4.2. Partially Reduced Oxygen Species. Rotating ring disc electrochemistry (RRDE) is used to estimate the amount of partially reduced oxygen species (PROS) produced due to incomplete O₂ reduction. In this technique any O₂^{•-} or O₂²⁻, that is, a 1e⁻ or 2e⁻ reduction produced in the modified Au working electrode is radially diffused, due to the hydrodynamic current created by the rotation, to the ring, which is held at 0.7 V, where these are oxidized back to O₂ (Scheme 4).^{82,85} This results in an oxidation current in the ring, and the ratio of the catalytic current of the disc (i_c) and the ring (i_r) yields the % of PROS produced. Note that if O₂ is reduced to H₂O, no current is detected in the ring.

The Fe "picket-fence" catalyst when bound to the imidazole linker produces 5% PROS, that is, 95% of the O₂ is reduced to H₂O. Alternatively, when the same catalyst is bound to thiolate almost twice the amount of PROS (10%) is produced (Table

5).⁸⁶ This reflects the trans effect of the thiolate ligand which leads to greater hydrolysis of the Fe^{III}–O₂⁻ and/or Fe^{III}–OOH species produced during O₂ reduction (Scheme 5) generating more PROS. The FeEs₄ catalyst produces 10% PROS when bound to the imidazole linker and 17% PROS when bound to the thiolate linker. The increase in PROS in the FeEs₄ catalyst relative to the Fe "picket-fence" catalyst (either imidazole or thiolate coordinated) reflects the greater hydrophilicity of the distal pocket in the FeEs₄ catalyst which increases the hydrolysis of the Fe^{III}–O₂⁻/Fe^{III}–OOH species produced on the electrode generating greater PROS.⁵³ Even for the FeEs₄ catalyst almost twice the amount of PROS is produced when bound to thiolate consistent with the result obtained with Fe "picket-fence". Note that the "push-effect" of thiolate is also reflected in the auto-oxidation rate of P450 enzyme when compared to Myoglobin (vide infra). The FeFc₄ catalyst which bears the hydrophilic distal pocket as well as the electron transfer site produces ~10% PROS for both imidazole and thiolate linkers. The presence of additional electron donors counter the trans effect of the thiolate ligand.

3.5. Substrate Oxidation. The CV of Fe "picket-fence" bound to the dithiol linker in pH 7 buffer containing 100 mM imidazole shows a well resolved Fe^{III}/Fe^{II} CV (Figure 13A, green). After one oxygen reduction cycle (i.e., a CV run between +0.5 V to –0.5 V in air saturated pH 7 buffer) 60% decay in the Fe^{III}/Fe^{II} current is observed (Figure 13A, orange). This implies that 60% of the catalyst has decayed possibly because of the production of highly oxidizing species during O₂ reduction. No such decay is observed when the same catalyst is bound to the imidazole linker (Supporting Information, Figure S10). Alternatively, when the FeFc₄ catalyst bound to the dithiol linker is used, that is, the catalyst bearing electron donor Fc groups, only 20% decay is observed (Figure 13B). This further supports the formation of a highly oxidizing intermediate during the oxygen reduction cycle, as the ferrocene group present reduces the lifetime of the reactive intermediate thus slowing down the decay of the catalyst, leading to greater stability of the catalyst. It is likely PROS produced during O₂ reduction may lead to catalytic decay. However, both the FeFc₄ catalyst and the Fe "picket fence" catalyst produce 10% PROS when bound to thiolate, but the former shows 20% decay whereas the latter shows 60% decay. Thus the decay is likely to be caused by an O₂ derived reactive species and not by PROS.

To chemically evaluate the possibility of formation of high valent intermediates during O₂ reduction by these iron porphyrin active sites on the electrodes, the O₂ reduction reactions are performed in the presence of K₄[Fe(CN)₆] using a RRDE setup. In these experiments the Pt ring is held at 0 V where it will reduce any [Fe(CN)₆]³⁻ formed to [Fe(CN)₆]⁴⁻. As the potential of the working electrode bearing the catalysts is gradually lowered and it starts to reduce O₂ (Figure 14, red and blue lines), the ring current simultaneously increases (Figure 14, dashed red and blue) suggesting concomitant oxidation of [Fe(CN)₆]⁴⁻ present in the solution to [Fe(CN)₆]³⁻. The formal potential of [Fe(CN)₆]^{3-/4-} is 0.24 V vs Ag/AgCl at pH 7 which is much higher than the potentials applied to the working of the Pt ring electrode during these experiments. Thus neither the working electrode or the Pt ring electrode can oxidize [Fe(CN)₆]⁴⁻ to [Fe(CN)₆]³⁻. Hence the iron porphyrin catalysts must be producing species with $E^{\circ} > 0.24$ V which is capable of oxidizing the [Fe(CN)₆]⁴⁻ present in the solution to [Fe(CN)₆]³⁻ which is then detected in the ring

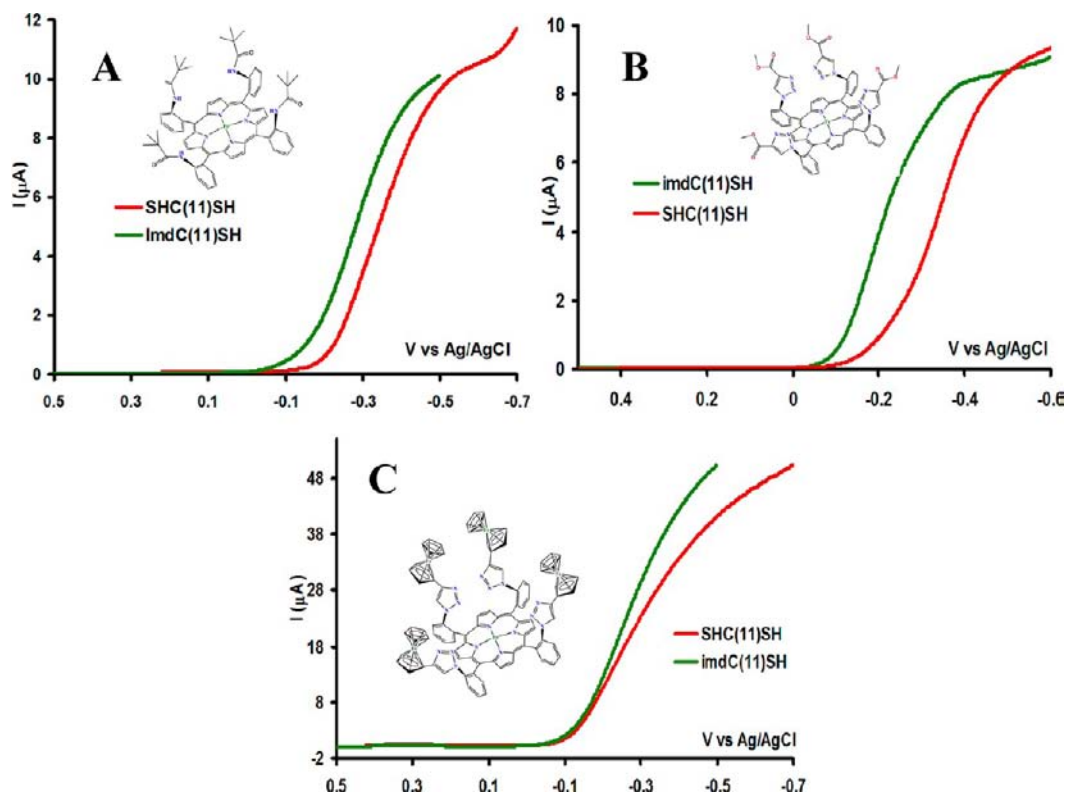


Figure 12. LSV data of Fe “picket-fence” (A), FeEs₄ (B), and FeFc₄ (C) in air saturated pH 7 buffer when attached to ImdC₁₁SH (green) and SHC₁₁SH (red) using Ag/AgCl as reference and Pt wire as counter electrodes.

Scheme 4. Schematic Representation of PROS Detection Mechanism by a RRDE Setup

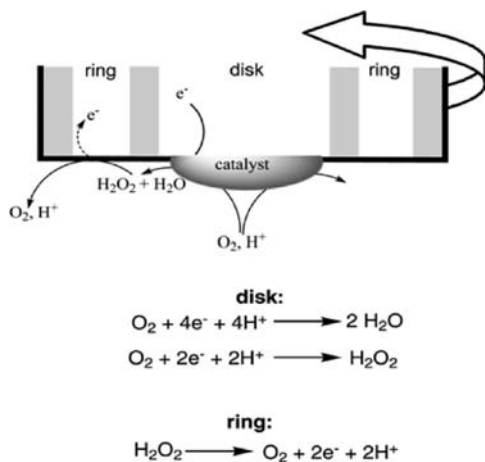
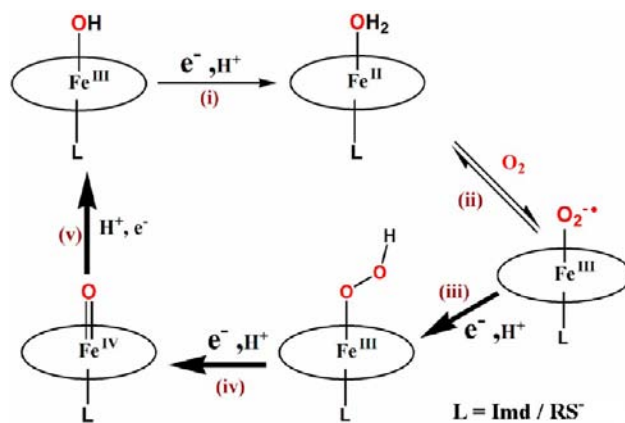


Table 5. PROS Values (%) with Different Linkers

catalyst	ImdC ₁₁ SH	SHC ₁₁ SH
Fe “picket-fence”	5 ± 1	9.8 ± 1
FeEs ₄	10 ± 2	17 ± 2
FeFc ₄	9 ± 1	10.5 ± 1

(Figure 14, dashed blue and red). Since the $E_{1/2}$ of Fe^{III/II} for iron porphyrin complexes are well below this value (Figure 9) the oxidation of [Fe(CN)₆]⁴⁻ indicates that species having oxidation states higher than +3 (Fe^{IV}=O of compound I type) are being generated on the electrode during O₂ reduction by iron porphyrin catalysts bound to both imidazole and thiol linkers. Note that a SAM covered Au electrode, that is, without

Scheme 5. Generic Oxygen Reduction Mechanism for Fe-Porphyrins



any catalyst, does not show any [Fe(CN)₆]³⁻ formation when swept over the same potential range. The amount of PROS (O₂⁻, H₂O₂) produced on these bioinspired electrodes (5–10%) is much less than the amount of [Fe(CN)₆]⁴⁻ oxidation observed (~15%). Thus these species can not account for the oxidation of [Fe(CN)₆]⁴⁻ to [Fe(CN)₆]³⁻ at these low potentials. In a control experiment, the oxidation of ferrocyanide to ferricyanide was monitored using a bare Au electrode as the working electrode. Bare Au disc (i.e., not covered by SAM) produces 55% PROS in pH 7. However 55% PROS produced oxidizes only about 17% ferrocyanide, that is, ~1/3rd. We think this is due to slow kinetics of oxidation of ferrocyanide to ferricyanide by H₂O₂ ~ 10⁻⁴ min⁻¹.⁸⁷ Thus, 5–10% PROS in these catalysts can only produce 1/3rd, that is,

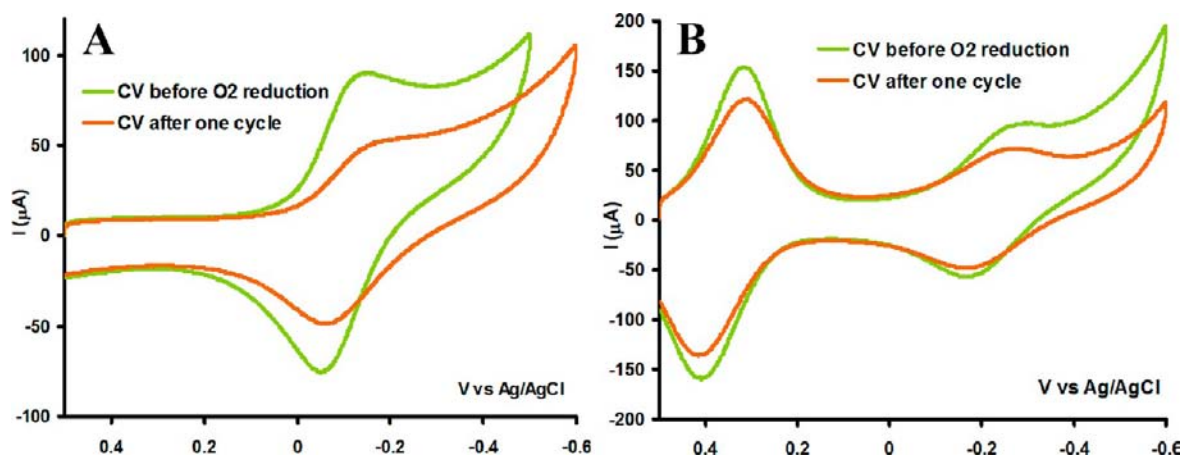


Figure 13. CV of Fe "picket-fence" (A) and FeFc₄ (B) attached to SHC₁₁SH linker in pH 7 buffer containing 100 mM imidazole before (light green) and after (orange) one O₂ reduction cycle in pH 7 buffer using Ag/AgCl as reference and Pt wire as counter electrodes.

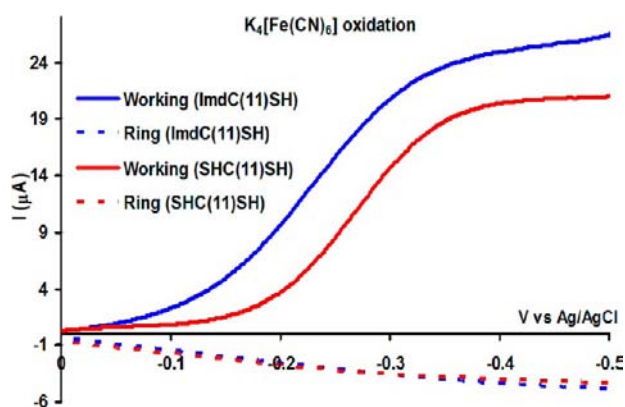


Figure 14. RRDE experiment of Fe "picket-fence" when bound to ImdC₁₁SH (blue) and SHC₁₁SH (red) linkers in pH 7 buffer containing 10 mM K₄[Fe(CN)₆] and ring held at 0 V using Ag/AgCl reference and Pt wire counter electrodes. The disc current is shown in bold line and ring current in dashed line.

1–3% ferricyanide. Hence we think the formation of 15% ferricyanide is likely due to oxidation of ferrocyanide by high-valent iron species formed during O₂ reduction.

Enthused by the possibility of formation of high-valent intermediates formed during O₂ reduction by the thiolate and imidazole ligated Fe "picket-fence" catalyst, the reactivity of these intermediates toward inert C–H bonds are investigated. Indeed, when substrates like cyclohexane and toluene are present in the aqueous buffer (saturated solutions) hydroxylations of very inert C–H bonds are observed (Table 6 and Supporting Information) in the thiolate bound Fe "picket-fence" surfaces. Gas chromatography (Figure S11 and S12, Supporting Information) and GC-MS of the products indicates that cyclohexane is oxidized to cyclohexanol and cyclohexanone with turnover numbers of 241 and 27, respectively.⁸⁸ Alternatively toluene, that bears both benzylic and aromatic

Table 6. C–H Bond Hydroxylation

substrate	product (TON)
cyclohexane	cyclohexanol (241)
	cyclohexanone (27)
toluene	benzyl alcohol (13)
	<i>p</i> -cresol (27)

C–H bonds, is oxidized to produce benzyl alcohol and *p*-cresol, that is, both benzylic and aromatic C–H bond hydroxylations are observed.⁸⁹ Interestingly, further oxidation of the hydroxylated products to ketones was not observed. This is possibly due to higher solubility of the hydroxylated products in water. This reactivity is unique to Fe "picket fence" porphyrin bound to thiolate. No detectable reaction is observed when thiolate is replaced by imidazole or when the hydrophobic Fe "picket-fence" is replaced by hydrophilic FeEs₄. These surfaces produce however significant amount of PROS (thiolate bound FeEs₄ produces 17% PROS). This suggests that the observed hydroxylations are catalyzed by metal centered high-valent species and not by PROS. Attempts to label the oxidized products by ¹⁸O, by using ¹⁸O₂ instead of ¹⁶O₂ during the formation of the high valent species, was not successful because of the very fast exchange rate between Fe^{IV}=¹⁸O and H₂¹⁶O.^{22,90,91}

One of the advantages of attaching catalysts to ligands immobilized on the surface is that these electrodes are recyclable. This is demonstrated by functionalizing a thiol linker bearing electrode with the Fe "picket-fence" catalyst (Supporting Information, Figure S15, green) and then, after utilizing this electrode to catalytically reduce O₂, washing off the electrode with dil. HCl (or any dilute acid). This protonates the axial thiolate ligand, and the Fe–S bond is cleaved. The free catalyst is then washed off and an electrode with no catalyst bound is generated which does not reduce O₂ (Supporting Information, Figure S15, cyan). This electrode is again successfully functionalized with Fe "picket-fence" and the catalytic O₂ reduction activity is gained back (Supporting Information, Figure S15, red). This allows recycling of electrodes bearing thiolate and imidazole linkers even after catalyst decay.

4. DISCUSSIONS

A combination of spectroscopic and electrochemical techniques indicates that dilute site-isolated active sites can be created where the axial ligand, thiolate or imidazole, is provided from the electrode. This approach has been previously demonstrated for imidazole and pyridine linkers and reduces the synthetic onus involved in making synthetic models.^{49,51} Conventionally synthesizing a Fe^{III}–SR porphyrin complex is complicated because of the $2\text{Fe}^{\text{III}} + 2\text{RS}^- \rightarrow 2\text{Fe}^{\text{II}} + \text{RSSR}$ process. However, this possibility is eliminated on very dilute surfaces

such as the ones used here as the thiolates are spatially separated and can not form disulfide dimers. Similarly, synthesis of iron porphyrins with covalently bound imidazole ligands are complicated by the formation of bridged dimers. Such a possibility is again reduced on a dilute surface employed here. SERRS and CV data allow determination of the nature of the active sites and the trans axial ligands. In spite of the fact that thiolate is a much stronger donor compared to imidazole, SERRS data show that the thiolate bound active sites are a mixture of five coordinated HS and six coordinated LS species while the imidazole bound active sites are all LS.⁷¹ In the low frequency region of SERRS data (Figure 5B and 6B) few additional bands are observed for thiolate axial ligands which may arise from the C–S stretching vibration, but conclusive assignments can not be made without isotope (S^{34}) labeling. The $Fe^{III/II}$ $E_{1/2}$ potential is determined to be more negative for the thiolate bound active site at pH 7. However, the $E_{1/2}$ of the imidazole and the thiolate bound active sites are difficult to compare at this stage as these sites vary in their spin states and also in the nature of the trans axial ligands (i.e., H_2O vs OH^-) which may significantly affect the $E_{1/2}$.⁹² The variation of the $E_{1/2}$ for the imidazole linker between pH 5–9 (~60 mV per pH unit) is suggestive of the presence of a proton coupled electron transfer process.⁷⁹ The oxidized ferric state is possibly bound to a hydroxide ligand and upon reduction accepts a neutral H_2O ligand; thus the reduction of the imidazole coordinated site requires a proton and hence its $E_{1/2}$ is pH dependent. Note that the protonation of the imidazole ligand does not occur in this pH range. The $E_{1/2}$ value for the thiolate linker is pH dependent below pH 6 and above pH 9 but remains independent in the range 6–9. These data are consistent with the presence of two pH equilibria for a thiolate bound iron porphyrin complex under aqueous environments. In the pH range 6–9 the axial ligands are thiolate and H_2O for both the oxidized and the reduced forms, and thus the $E_{1/2}$ remains pH independent.⁹³ Below pH 6 an RS^-/RSH equilibrium and above pH 9 an OH^-/H_2O equilibrium exists, respectively. Both the processes require protonation and are thus pH dependent. However, like some P450 active sites, in the presence of a strong trans axial ligand like CO, the pK_a of the thiolate ligand is raised and it gets protonated at pH 7.⁶⁴ Notably the $E_{1/2}$ values obtained at various pHs have a contribution from both the HS and the LS components as observed in SERRS with the HS species being the major one. Similar pH dependence of $Fe^{III/II}$ $E_{1/2}$ is reported for some P450 family of enzymes although the analysis there is complicated by a synchronous change in spin state of the iron center.^{94,95}

The pH dependence of the $Fe^{III/II}$ $E_{1/2}$ suggest that the thiolate axial ligand raises the pK_a of the trans aquo ligand such that it remains H_2O for the oxidized ferric site even at pHs as high as 9. This is very similar to the very high pK_a observed for the trans H_2O ligand present in the Cytochrome P450 active site.⁹⁶ Alternatively, pK_a of H_2O ligand bound to iron porphyrin complexes and active sites bearing coordinated imidazole ligand vary from 6 to 8 depending on the environment.⁸⁰ In iron porphyrin complexes, bearing no additional redox active site, the amount of PROS detected with a thiolate linker is twice of that detected with an imidazole linker irrespective of the porphyrin architecture. PROS result from the hydrolysis of $Fe^{II}-O_2/Fe^{III}-OOH$ species and thus may reflect the higher “push-effect” of the trans thiolate ligand.¹⁰ In the presence of triazole groups in the distal pocket (in case of $FeEs_4$) greater amount of PROS is produced for both the thiolate and the

imidazole linkers. This could be due to hydrophobicity of the picket fence architecture and/or stabilization of the $Fe-O_2$ adduct due to hydrogen bonding from the amide groups. However the thiolate still produces ~2 times more PROS relative to the imidazole linker. The auto-oxidation rate of P450 enzyme is $20 s^{-1}$ whereas that of myoglobin is $10^{-5} s^{-1}$.^{97–99} Thus the higher PROS generation of the thiolate ligand is in general agreement with the higher rate of auto-oxidation in cytochrome P450 relative to myoglobin. However, in our system, the PROS vary by a factor of 2 when in the enzymes the first order auto-oxidation rates vary by 10^6 . Thus during steady state the push-effect of the thiolate possibly significantly enhances the rate of O–O bond cleavage to compete with auto-oxidation. In the case of $FeFc_4$ the presence of an extra reducing center on the porphyrin distal structure minimizes this effect.

Several mimics of Cytochrome P450 are available in literature, but almost all are unstable in air.^{52,100–102} There are only very few reports of these thiolate bound active sites which are stable in air but neither has explored O_2 activation.^{103,104} Reports do exist where thiolate bound systems have activated C–H bonds using H_2O_2 , m-CPBA.²⁷ These systems are not equivalent to Cyt P450 which uses molecular O_2 . Here we report, for the first time, C–H hydroxylation by a thiolate bound porphyrin using molecular O_2 , a function so far attributed only to Cytochrome P450. The thiolate ligated Fe “picket-fence” is very reactive and decays fast during O_2 reduction. This suggests formation of highly reactive, possibly high-valent, intermediates during O_2 reduction. These highly reactive intermediates have been used to oxidize inert C–H bonds. Cyclohexane (BDE = 99.3 kcal/mol)²³ is oxidized to cyclohexanol and cyclohexanone, and toluene (BDE, benzylic = 89.9 kcal/mol, aromatic = 85 kcal/mol)¹⁰⁵ is oxidized to cresol and benzyl alcohol. These oxidations occur in pH 7 buffer (saturated with the substrate) at room temperature and using molecular O_2 . Turnover numbers as high as 200 are estimated. The results indicate that while diffusion of the hydrophobic substrate to the hydrophobic distal environment is favored, further oxidation of the hydroxylated products is not observed possibly because of higher solubility of these complexes in aqueous medium which diffuses them out into the bulk solvent and away from the reaction center localized on the hydrophobic monolayer (Figure S16, Supporting Information). When coordinated to the imidazole linker, the iron porphyrin site does produce $Fe(IV)$ species (likely to be $Fe^{IV}=O$) during O_2 reduction which can oxidize $[Fe(CN)_6]^{4-}$ to $[Fe(CN)_6]^{3-}$. However this species is not catalytically competent to hydroxylate C–H bonds. Further, no C–H bond hydroxylations were observed when a porphyrin catalyst with a hydrophilic distal cavity was used. This is likely because the hydrophobic substrates used here do not dock in these hydrophilic distal cavities which is possibly essential for reactivity. The hydrophobic distal structure of “picket-fence” porphyrin is ideal for this purpose. Note that the C–H bond hydroxylation may be catalyzed by high-valent reactive species formed via a peroxide shunt (from the PROS formed) or during reduction of molecular oxygen. RRDE data indicate that the $FeEs_4$ complex bound to a thiolate ligand produce maximum PROS (17%), but it shows no C–H hydroxylation. Similarly, neither of the imidazole bound iron porphyrin complexes shows any detectable activity in spite of producing detectable PROS. Thus O_2 derived high-valent species, that is,

$\text{Fe}^{\text{IV}}=\text{O}$ and not PROS, are likely to catalyze the C–H bond hydroxylation observed here.

Catalytic C–H bond hydroxylation using molecular O_2 has been a long-term goal for chemists. C–H bond hydroxylation is a $2e^-$ oxidation while the reduction of molecular O_2 requires $4e^-$. In Cytochrome P450 the two additional electrons needed during substrate hydroxylation using O_2 are provided by a reductase component (flavin or ferredoxin). These reduced active sites, in spite of having very low E° , do not reduce O_2 as they are protected inside a protein environment. A formidable challenge involved in making synthetic catalysts that can catalyze the same reaction is to provide electrons to the active site but not directly to molecular O_2 (a reducing agent capable of reducing P450 type complexes, that is, $E^\circ < -0.5$ V, may, and often will, reduce O_2 directly). In our system the electrode acts as the reductase component by providing electrons to the active site during turnover. Here electrons do not directly reduce O_2 as it is insulated by the SAM, that is, SAM provides the insulation analogous to the environment in a protein.

Previous attempts of electrochemically oxidizing organic alcohols used Rh porphyrins to generate high-valent species in aqueous solutions by applying high potentials (>1 V) on the electrodes.^{106–108} In these attempts the oxidizing equivalents are provided by the electrode and not by molecular O_2 . There are some inspiring early reports where high-valent oxo species of Mn or Fe porphyrins were generated electrochemically in organic solvents or immobilized in electrodes and were used to activate C–H bonds using molecular O_2 .^{109–112} These works report high turnover numbers (TON) and very high Faradaic yields (FY). Here, by mimicking the thiolate ligation and hydrophobic substrate binding pocket of “picket-fence” porphyrins, we are able to oxidize C–H bonds using molecular O_2 in aqueous solvents using a similar approach. In our case though TON is almost similar to these reports, FY is about $\sim 10\%$. In the current approach there is always a competition between reaction of the high-valent intermediates with the substrate (catalytic process, Scheme 6, blue arrow) and reduction of these by electron transfer from the electrodes (Scheme 6, green arrow) leading to $4e^-/4\text{H}^+$ O_2 reduction. This compromises the FY of this process.¹¹³ The electron transfer rate can be retarded by increasing the chain length of the thiols used. This should, in principle, increase the lifetime of the

reactive species on the electrode and hence increase the probability of the catalytic process.

Finally, a key advantage of these electrodes is that they can be reversibly constructed which minimizes the effort and time of reloading. An attachment via an irreversible covalent bond formation or through thin layer deposition is also well-known. However, in those cases the electrode and the monolayer become dysfunctional as the catalyst decays. Alternatively, the metal ligand bonds are easily cleaved via protonation. This allows the metal catalyst to be easily removed after washing with dilute acid without affecting the monolayer.

5. CONCLUSION

In summary, thiolate and imidazole bound site-isolated active sites are created on self assembled monolayers. These easy to construct recyclable electrodes can activate molecular O_2 in pH 7 and generate high-valent species in the process which can catalyze C–H bond hydroxylations at room temperature. Turnover number as high as 200 is estimated for oxidation of cyclohexane to cyclohexanol using molecular O_2 .

■ ASSOCIATED CONTENT

Supporting Information

Synthetic details, characterization data of the synthesized compounds and oxidized products, CV, SERRS, and absorption data. This material is available free of charge via the Internet at <http://pubs.acs.org>.

■ AUTHOR INFORMATION

Corresponding Author

*E-mail: icad@iacs.res.in.

Notes

The authors declare no competing financial interest.

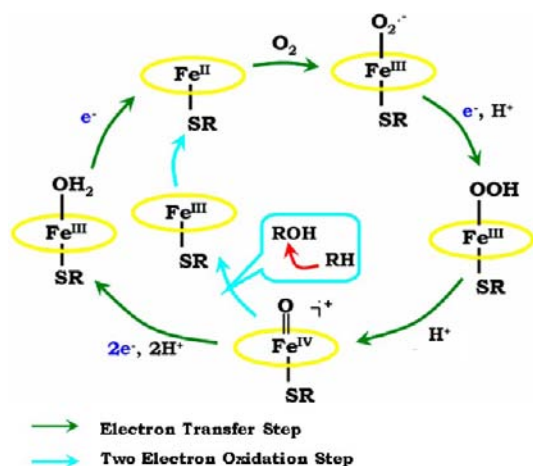
■ ACKNOWLEDGMENTS

This work was funded by the Department of Science and Technology, India, Grant DST/SR/IC-35-2009. K.S. and S.C. acknowledge CSIR-SRF and CSIR-JRF fellowships respectively. S.S. and S.B. acknowledge the integrated Ph.D. program of IACS. A.D. acknowledges Prof. S. Bhattacharya of Jadavpur University for GC-MS measurements.

■ REFERENCES

- (1) Riggs, A. F. *Curr. Opin. Struct. Biol.* **1991**, *1*, 915.
- (2) Møller, J. K. S.; Skibsted, L. H. *Chem. Rev.* **2002**, *102*, 1167.
- (3) Flögel, U.; Merx, M. W.; Gödecke, A.; Decking, U. K. M.; Schrader, J. r. *Proc. Natl. Acad. Sci. U. S. A.* **2001**, *98*, 735.
- (4) Kim, E.; Chufan, E. E.; Kamaraj, K.; Karlin, K. D. *Chem. Rev.* **2004**, *104*, 1077.
- (5) Denisov, I. G.; Makris, T. M.; Sligar, S. G.; Schlichting, I. *Chem. Rev.* **2005**, *105*, 2253.
- (6) Ferguson-Miller, S.; Babcock, G. T. *Chem. Rev.* **1996**, *96*, 2889.
- (7) Sono, M.; Roach, M. P.; Coulter, E. D.; Dawson, J. H. *Chem. Rev.* **1996**, *96*, 2841.
- (8) Green, M. T.; Dawson, J. H.; Gray, H. B. *Science* **2004**, *304*, 1653.
- (9) Meunier, B.; de Visser, S. I. P.; Shaik, S. *Chem. Rev.* **2004**, *104*, 3947.
- (10) Dawson, J. H.; Sono, M. *Chem. Rev.* **1987**, *87*, 1255.
- (11) Mak, L. H.; Sadeghi, S. J.; Fantuzzi, A.; Gilardi, G. *Anal. Chem.* **2010**, *82*, 5357.
- (12) Sadeghi, S. J.; Fantuzzi, A.; Gilardi, G. *Biochim. Biophys. Acta, Proteins Proteomics* **2011**, *1814*, 237.

Scheme 6. Schematic Representation of the Competing Reactions on a Bio-Inspired Electrode



- (13) van der Felt, C.; Hindoyan, K.; Choi, K.; Javdan, N.; Goldman, P.; Bustos, R.; Star, A. G.; Hunter, B. M.; Hill, M. G.; Nersissian, A.; Udit, A. K. *J. Inorg. Biochem.* **2011**, *105*, 1350.
- (14) Higuchi, T.; Uzu, S.; Hirobe, M. *J. Am. Chem. Soc.* **1990**, *112*, 7051.
- (15) Ueyama, N.; Nishikawa, N.; Yamada, Y.; Okamura, T.-a.; Nakamura, A. *J. Am. Chem. Soc.* **1996**, *118*, 12826.
- (16) Ueno, T.; Nishikawa, N.; Moriyama, S.; Adachi, S.; Lee, K.; Okamura, T.-a.; Ueyama, N.; Nakamura, A. *Inorg. Chem.* **1999**, *38*, 1199.
- (17) Costas, M.; Mehn, M. P.; Jensen, M. P.; Que, L. *Chem. Rev.* **2004**, *104*, 939.
- (18) Mirica, L. M.; Vance, M.; Rudd, D. J.; Hedman, B.; Hodgson, K. O.; Solomon, E. I.; Stack, T. D. P. *Science* **2005**, *308*, 1890.
- (19) Collman, J. P.; Dey, A.; Yang, Y.; Ghosh, S.; Decréau, R. A. *Proc. Natl. Acad. Sci. U. S. A.* **2009**, *106*, 10528.
- (20) Nam, W.; Lim, M. H.; Moon, S. K.; Kim, C. *J. Am. Chem. Soc.* **2000**, *122*, 10805.
- (21) Pires, S. M. G.; Paula, R. D.; Simoes, M. M. Q.; Silva, A. M. S.; Domingues, M. R. M.; Santos, I. C. M. S.; Vargas, M. D.; Ferreira, V. F.; Neves, M. G. P. M. S.; Cavaleiro, J. A. S. *RSC Advances* **2011**, *1*, 1195.
- (22) Nam, W.; Park, S.-E.; Lim, I. K.; Lim, M. H.; Hong, J.; Kim, J. *J. Am. Chem. Soc.* **2003**, *125*, 14674.
- (23) Kaizer, J. z.; Klinker, E. J.; Oh, N. Y.; Rohde, J.-U.; Song, W. J.; Stubna, A.; Kim, J.; Münck, E.; Nam, W.; Que, L. *J. Am. Chem. Soc.* **2004**, *126*, 472.
- (24) Cho, K.-B.; Chen, H.; Janardanan, D.; de Visser, S. P.; Shaik, S.; Nam, W. *Chem. Commun.* **2012**, *48*, 2189.
- (25) Seo, M. S.; Kim, N. H.; Cho, K.-B.; So, J. E.; Park, S. K.; Clemancey, M.; Garcia-Serres, R.; Latour, J.-M.; Shaik, S.; Nam, W. *Chem. Sci.* **2011**, *2*, 1039.
- (26) Liu, W.; Groves, J. T. *J. Am. Chem. Soc.* **2010**, *132*, 12847.
- (27) Bell, S. R.; Groves, J. T. *J. Am. Chem. Soc.* **2009**, *131*, 9640.
- (28) Shook, R. L.; Borovik, A. S. *Chem. Commun.* **2008**, 6095.
- (29) Wu, X.; Seo, M. S.; Davis, K. M.; Lee, Y.-M.; Chen, J.; Cho, K.-B.; Pushkar, Y. N.; Nam, W. *J. Am. Chem. Soc.* **2011**, *133*, 20088.
- (30) Cho, J.; Jeon, S.; Wilson, S. A.; Liu, L. V.; Kang, E. A.; Braymer, J. J.; Lim, M. H.; Hedman, B.; Hodgson, K. O.; Valentine, J. S.; Solomon, E. I.; Nam, W. *Nature* **2011**, *478*, 502.
- (31) Lee, Y.-M.; Hong, S.; Morimoto, Y.; Shin, W.; Fukuzumi, S.; Nam, W. *J. Am. Chem. Soc.* **2010**, *132*, 10668.
- (32) Mukherjee, A.; Cranswick, M. A.; Chakrabarti, M.; Paine, T. K.; Fujisawa, K.; Münck, E.; Que, L., Jr. *Inorg. Chem.* **2010**, *49*, 3618.
- (33) Martinho, M.; Blain, G.; Banse, F. *Dalton Trans.* **2010**, *39*, 1630.
- (34) Nam, W. *Acc. Chem. Res.* **2007**, *40*, 522.
- (35) Lee, D.; Pierce, B.; Krebs, C.; Hendrich, M. P.; Huynh, B. H.; Lippard, S. J. *J. Am. Chem. Soc.* **2002**, *124*, 3993.
- (36) Shook, R. L.; Gunderson, W. A.; Greaves, J.; Ziller, J. W.; Hendrich, M. P.; Borovik, A. S. *J. Am. Chem. Soc.* **2008**, *130*, 8888.
- (37) Friedle, S.; Reisner, E.; Lippard, S. J. *Chem. Soc. Rev.* **2010**, *39*, 2768.
- (38) Love, J. C.; Estroff, L. A.; Kriebel, J. K.; Nuzzo, R. G.; Whitesides, G. M. *Chem. Rev.* **2005**, *105*, 1103.
- (39) Stupp, S. I. *Chem. Rev.* **2005**, *105*, 1023.
- (40) Chidsey, C. E. D. *Science* **1991**, *251*, 919.
- (41) Prime, K. L.; Whitesides, G. M. *Science* **1991**, *252*, 1164.
- (42) Yokoyama, K.; Leigh, B. S.; Sheng, Y.; Niki, K.; Nakamura, N.; Ohno, H.; Winkler, J. R.; Gray, H. B.; Richards, J. H. *Inorg. Chim. Acta* **2008**, *361*, 1095.
- (43) Fujita, K.; Nakamura, N.; Ohno, H.; Leigh, B. S.; Niki, K.; Gray, H. B.; Richards, J. H. *J. Am. Chem. Soc.* **2004**, *126*, 13954.
- (44) Udit, A. K.; Hollingsworth, W.; Choi, K. *Bioconjugate Chem.* **2010**, *21*, 399.
- (45) Albrecht, T.; Li, W.; Ulstrup, J.; Haehnel, W.; Hildebrandt, P. *ChemPhysChem* **2005**, *6*, 961.
- (46) Collman, J. P.; Decreau, R. A. *Chem. Commun.* **2008**, 5065.
- (47) Collman, J. P.; Devaraj, N. K.; Eberspacher, T. P. A.; Chidsey, C. E. D. *Langmuir* **2006**, *22*, 2457.
- (48) Mukherjee, S.; Sengupta, K.; Das, M.; Jana, S.; Dey, A. *J. Biol. Inorg. Chem.* **2012**, *17*, 1009.
- (49) Offord, D. A.; Sachs, S. B.; Ennis, M. S.; Eberspacher, T. A.; Griffin, J. H.; Chidsey, C. E. D.; Collman, J. P. *J. Am. Chem. Soc.* **1998**, *120*, 4478.
- (50) Eberspacher, T. A.; Collman, J. P.; Chidsey, C. E. D.; Donohue, D. L.; Van Ryswyk, H. *Langmuir* **2003**, *19*, 3814.
- (51) Vecchi, A.; Gatto, E.; Floris, B.; Conte, V.; Venanzi, M.; Nemykin, V. N.; Galloni, P. *Chem. Commun.* **2012**, *48*, 5145.
- (52) Collman, J. P.; Gagne, R. R.; Reed, C.; Halbert, T. R.; Lang, G.; Robinson, W. T. *J. Am. Chem. Soc.* **1975**, *97*, 1427.
- (53) Samanta, S.; Sengupta, K.; Mittra, K.; Bandyopadhyay, S.; Dey, A. *Chem. Commun.* **2012**, *48*, 7631.
- (54) Mittra, K.; Chatterjee, S.; Samanta, S.; Sengupta, K.; Bhattacharjee, H.; Dey, A. *Chem. Commun.* **2012**, *48*, 10535–.
- (55) Lower concentrations than this did not result in good SAM.
- (56) Pramanik, D.; Sengupta, K.; Mukherjee, S.; Dey, S. G.; Dey, A. *J. Am. Chem. Soc.* **2012**, *134*, 12180.
- (57) Zhang, Y.; Wilson, G. S. *J. Electroanal. Chem.* **1993**, *345*, 253.
- (58) Bulovas, A. T., Z.; Niaura, G.; Kažemėkaitė, M.; Marcinkevičienė, L.; Bachmatova, I. M., R.; Razumas, V. *Chemija* **2007**, *18*, 9.
- (59) Hildebrandt, P.; Macor, K. A.; Czernuszewicz, R. S. *J. Raman Spectrosc.* **1988**, *19*, 65.
- (60) Sharma, B.; F., R. R.; Henry, A. I.; Ringe, E.; Van Duyne, R. P. *Mater. Today* **2012**, *15*, 16.
- (61) Murgida, D. H.; Hildebrandt, P. *Chem. Soc. Rev.* **2008**, *37*, 937.
- (62) The λ_{\max} of the Soret were determined by taking a first derivative of the spectrum (derivative = 0 at maximum). However, the data on the reduced imidazole bound complex did not offer a clean maximum using the first derivative. In that case the maximum was approximated.
- (63) Tsuchida, E.; Komatsu, T.; Arai, K.; Nishide, H. *J. Chem. Soc., Dalton Trans.* **1993**, 2465.
- (64) Udit, A. K.; Hagen, K. D.; Goldman, P. J.; Star, A.; Gillan, J. M.; Gray, H. B.; Hill, M. G. *J. Am. Chem. Soc.* **2006**, *128*, 10320.
- (65) Smith, A. T.; Su, Y.; Stevens, D. J.; Majtan, T.; Kraus, J. P.; Burstyn, J. N. *Biochemistry* **2012**, *51*, 6360.
- (66) Dawson, J. H.; Andersson, L. A.; Sono, M. *J. Biol. Chem.* **1982**, *257*, 3606.
- (67) Zhao, J.; Das, A.; Schatz, G. C.; Sligar, S. G.; Van Duyne, R. P. *J. Phys. Chem. C* **2008**, *112*, 13084.
- (68) Das, A.; Zhao, J.; Schatz, G. C.; Sligar, S. G.; Van Duyne, R. P. *Anal. Chem.* **2009**, *81*, 3754.
- (69) Zhao, J.; Das, A.; Zhang, X.; Schatz, G. C.; Sligar, S. G.; Van Duyne, R. P. *J. Am. Chem. Soc.* **2006**, *128*, 11004.
- (70) Hashimoto, S.; Mizutani, Y.; Tatsuno, Y.; Kitagawa, T. *J. Am. Chem. Soc.* **1991**, *113*, 6542.
- (71) Burke, J. M.; Kincaid, J. R.; Peters, S.; Gagne, R. R.; Collman, J. P.; Spiro, T. G. *J. Am. Chem. Soc.* **1978**, *100*, 6083.
- (72) Das, P. K.; Chatterjee, S.; Samanta, S.; Dey, A. *Inorg. Chem.* **2012**, *51* (20), 10704–.
- (73) The Fe-S vibration for the $S = 1/2$ species is reported to be $\sim 390\text{ cm}^{-1}$ which overlaps with the strong ν_8 band.
- (74) Meinhold, P.; Peters, M. W.; Hartwick, A.; Hernandez, A. R.; Arnold, F. H. *Adv. Synth. Catal.* **2006**, *348*, 763.
- (75) Lewis, J. C.; Coelho, P. S.; Arnold, F. H. *Chem. Soc. Rev.* **2011**, *40*, 2003.
- (76) The CV waves retain their nature and the $E_{1/2}$ values remain unchanged even after background correction (Supporting Information, Figure S8).
- (77) This is also indicated from the UV-vis data. Note that the coverages obtained from both the methods are in agreement.
- (78) Costentin, C.; Robert, M.; Saveant, J.-M. *Chem. Rev.* **2010**, *110*, PR1.
- (79) Hammes-Schiffer, S.; Stuchebrukhov, A. A. *Chem. Rev.* **2010**, *110*, 6939.
- (80) Pramanik, D.; Dey, S. G. *J. Am. Chem. Soc.* **2011**, *133*, 81.

(81) FeFc₄ complex dissociates in the presence of 100 mM imidazole in the buffer. So no CV of imidazole bound FeFc₄ attached to the Imidazole linker could be recorded.

(82) Collman, J. P.; Fu, L.; Herrmann, P. C.; Zhang, X. *Science* **1997**, *275*, 949.

(83) Chang, C. J.; Loh, Z.-H.; Shi, C.; Anson, F. C.; Nocera, D. G. *J. Am. Chem. Soc.* **2004**, *126*, 10013.

(84) Shi, C.; Anson, F. C. *Inorg. Chem.* **1990**, *29*, 4298.

(85) Bard, A. J.; Faulkner, L. R. *Electrochemical Methods*; J. Wiley: New York, 1980; p 300.

(86) The reaction of decomposed porphyrin with oxygen cannot be ruled out and may also be a reason for PROS generation.

(87) Kistiakowsky, W. Z. *Physik. Chem.* **1900**, *35*, 431.

(88) The turnover numbers are calculated by obtaining the respective concentration of the oxidized samples from the titration curve of the standards. (Supporting Information, Figure S13 and S14).

(89) In addition to the hydroxylated products a non polar product is observed (major product), the identity of which could not be confirmed at this point.

(90) Nam, W.; Valentine, J. S. *J. Am. Chem. Soc.* **1993**, *115*, 1772.

(91) Goh, Y. M.; Nam, W. *Inorg. Chem.* **1999**, *38*, 914.

(92) Sligar, S. G. *Biochemistry* **1976**, *15*, 5399.

(93) In page 36 where the equilibrium has been mentioned the trans ligand is H₂O so it remains as S- at pH 7. But when the trans ligand is CO (as in UV-vis) the pK_a shifts higher and so the linker remains protonated, i.e., as SH.

(94) Makino, R.; Chiang, R.; Hager, L. P. *Biochemistry* **1976**, *15*, 4748.

(95) Sligar, S. G.; Gunsalus, I. C. *Biochemistry* **1979**, *18*, 2290.

(96) Goldfarb, D.; Bernardo, M.; Thomann, H.; Kroneck, P. M. H.; Ullrich, V. *J. Am. Chem. Soc.* **1996**, *118*, 2686.

(97) Sligar, S. G.; Lipscomb, J. D.; Debrunner, P. G.; Gunsalus, I. C. *Biochem. Biophys. Res. Commun.* **1974**, *61*, 290.

(98) Denisov, I. G.; Grinkova, Y. V.; Baas, B. J.; Sligar, S. G. *J. Biol. Chem.* **2006**, *281*, 23313.

(99) Brantley, R. E.; Smerdon, S. J.; Wilkinson, A. J.; Singleton, E. W.; Olson, J. S. *J. Biol. Chem.* **1993**, *268*, 6995.

(100) Chang, C. K.; Dolphin, D. J. *Am. Chem. Soc.* **1975**, *97*, 5948.

(101) Traylor, T. G.; Mincey, T. C.; Berzini, A. P. *J. Am. Chem. Soc.* **1981**, *103*, 7084.

(102) Tani, F.; Matsu-ura, M.; Nakayama, S.; Naruta, Y. *Coord. Chem. Rev.* **2002**, *226*, 219.

(103) Suzuki, N.; Higuchi, T.; Urano, Y.; Kikuchi, K.; Uekusa, H.; Ohashi, Y.; Uchida, T.; Kitagawa, T.; Nagano, T. *J. Am. Chem. Soc.* **1999**, *121*, 11571.

(104) Das, P. K.; Chatterjee, S.; Samanta, S.; Dey, A. *Inorg. Chem.* **2012**, *51*, 10704.

(105) Wu, Y.-D.; Wong, C.-L.; Chan, K. W. K.; Ji, G.-Z.; Jiang, X.-K. *J. Org. Chem.* **1996**, *61*, 746.

(106) Yamazaki, S.-i.; Yao, M.; Fujiwara, N.; Siroma, Z.; Yasuda, K.; Ioroi, T. *Chem. Commun.* **2012**, *48*, 4353.

(107) Liu, L.; Yu, M.; Wayland, B. B.; Fu, X. *Chem. Commun.* **2010**, *46*, 6353.

(108) Elouarzaki, K.; Le Goff, A.; Holzinger, M.; Thery, J.; Cosnier, S. *J. Am. Chem. Soc.* **2012**, *134*, 14078.

(109) Creager, S. E.; Murray, R. W. *Inorg. Chem.* **1987**, *26*, 2612.

(110) Creager, S. E.; Raybuck, S. A.; Murray, R. W. *J. Am. Chem. Soc.* **1986**, *108*, 4225.

(111) Guo, C.-C.; Huang, G.; Zhang, X.-B.; Guo, D.-C. *Appl. Catal., A* **2003**, *247*, 261.

(112) Nouri-Nigjeh, E.; Bischoff, R.; Bruins, A. P.; Permentier, H. P. *Curr. Drug Metab.* **2011**, *12*, 359.

(113) It is surprising that the previous reports show high FY in the presence of O₂ and H⁺ in the medium as all of these porphyrins are known to electrocatalytically reduce O₂ in organic solvents.